J Biomol NMR (2007) 37:179–185
DOI 10.1007/s10858-006-9108-8

ARTICLE

Pairwise NMR experiments for the determination of protein backbone dihedral angle Φ based on cross-correlated spin relaxation

Hideo Takahashi · Ichio Shimada

Received: 2 August 2006 / Accepted: 16 October 2006 / Published online: 20 January 2007
© Springer Science+Business Media B.V. 2007

Abstract Novel cross-correlated spin relaxation (CCR) experiments are described, which measure pairwise CCR rates for obtaining peptide dihedral angles Φ. The experiments utilize intra-HNCA type coherence transfer to refocus 2-bond $J_{NC\alpha}$ coupling evolution and generate the $N(i)$–$C^{\alpha}(i)$ or $C'(i-1)$–$C^{\alpha}(i)$ multiple quantum coherences which are required for measuring the desired CCR rates. The contribution from other coherences is also discussed and an appropriate setting of the evolution delays is presented. These CCR experiments were applied to ^{15}N- and ^{13}C-labeled human ubiquitin. The relevant CCR rates showed a high degree of correlation with the Φ angles observed in the X-ray structure. By utilizing these CCR experiments in combination with those previously established for obtaining dihedral angle Ψ, we can determine high resolution structures of peptides that bind weakly to large target molecules.

Keywords Chemical shift anisotropy · Cross-correlated relaxation · Dihedral angle · Dipole–dipole interaction · Intra-HNCA · Structure determination

H. Takahashi (✉) · I. Shimada
Biological Information Research Center (BIRC), National Institute of Advanced Industrial Science and Technology (AIST), Aomi 2-41-6, Koto-ku, Tokyo 135-0064, Japan
e-mail: hid@jbirc.aist.go.jp

I. Shimada
Graduate School of Pharmaceutical Sciences, The University of Tokyo, Hongo 7-3-1, Bunkyo-ku, Tokyo 113-0033, Japan
e-mail: shimada@iw-nmr.f.u-tokyo.ac.jp

Introduction

Cross-correlated spin relaxation (CCR) between two different relaxation mechanisms can provide valuable information about macromolecular structure and dynamics. Reif et al. have developed a method utilizing CCR between interresidual dipolar fields of ^{15}N–^{1}H (residue $i+1$) and $^{13}C^{\alpha}$–$^{1}H^{\alpha}$ (residue i) internuclear vectors, denoted as $\Gamma_{H\alpha C\alpha,HN}(\Psi)$ (Fig. 1a), to measure the backbone dihedral angle Ψ of proteins (Reif et al. 1997). However, since a single relaxation rate can give rise to a multiplicity of dihedral angles, there is a limitation in the use of CCR in angle determination. Therefore, Yang et al. developed an alternative experiment to measure Ψ, based on CCR between intraresidual $^{13}C^{\alpha}$–$^{1}H^{\alpha}$ dipolar and $^{13}C'$ (carbonyl) chemical shift anisotropy (CSA) relaxation mechanisms, $\Gamma_{H\alpha C\alpha,C'}(\Psi)$ (Fig. 1b: Yang et al. 1997). It has been shown that the number of possible Ψ angles can be considerably reduced by combining measurements from these two experiments. This can lead to unambiguous determination of dihedral angles in favorable cases (Yang and Kay 1998). Several CCR experiments were developed to determine $\Gamma_{H\alpha C\alpha,HN}(\Psi)$ and $\Gamma_{H\alpha C\alpha,C'}(\Psi)$ by utilizing HN(CO)CA type coherence transfer. Among those experiments, it is suggested that quantitative Γ methods (Pelupessy et al. 1999a; Chiarparin et al. 1999; Sprangers et al. 2000) by complementary two-dimensional measurements are preferred from a sensitivity viewpoint (Carlomagno and Griesinger 2000).

In the case of the backbone dihedral angle Φ, a similar strategy is followed, which utilizes intraresidual ^{15}N–^{1}H dipolar/$^{13}C^{\alpha}$–$^{1}H^{\alpha}$ dipolar CCR, $\Gamma_{HN,H\alpha C\alpha}(\Phi)$ (Fig. 1c: Pelupessy et al. 1999b; Kloiber et al. 2002) and

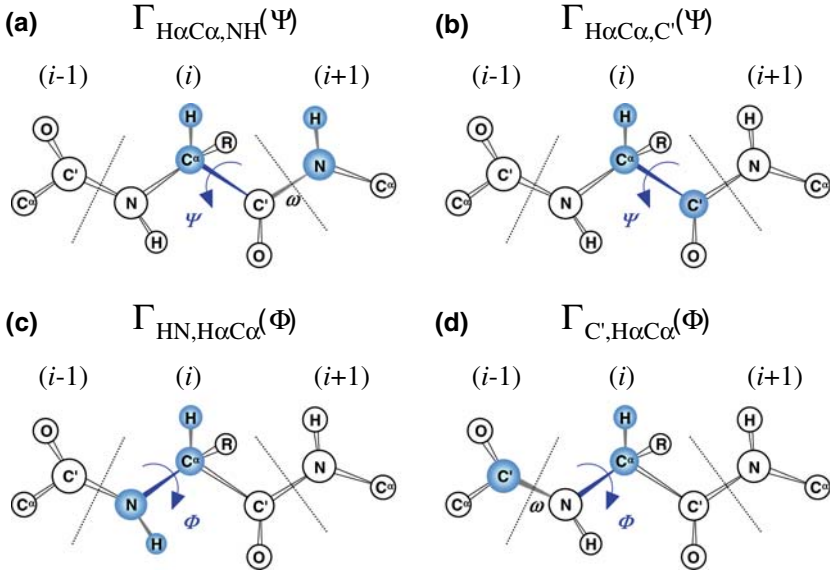

Fig. 1 Schematic representation of the four cross-correlated spin relaxation rates associated with the determination of backbone dihedral angles Φ and Ψ. (**a**) $\Gamma_{H\alpha C\alpha,HN}(\Psi)$; (**b**) $\Gamma_{H\alpha C\alpha,C'}(\Psi)$; (**c**) $\Gamma_{HN,H\alpha C\alpha}(\Phi)$; (**d**) $\Gamma_{C',H\alpha C\alpha}(\Phi)$

interresidual $^{13}C'(i-1)$ CSA/$^{13}C^{\alpha}(i)$–$^{1}H^{\alpha}(i)$ dipolar CCR, $\Gamma_{C',H\alpha C\alpha}(\Phi)$ (Fig. 1d: Kloiber and Konrat 2000). Since the pulse sequences for these experiments utilize or partially utilize HNCA type coherence transfer, the evolution of $^{1}J_{NC\alpha}$ and $^{2}J_{NC\alpha}$ spin couplings are active during the ^{15}N evolution period. These couplings hamper a simple derivation of these CCR rates. Therefore, in order to obtain $\Gamma_{HN,H\alpha C\alpha}(\Phi)$ and $\Gamma_{C',H\alpha C\alpha}(\Phi)$, time-consuming 3D experiments were performed (Pelupessy et al. 1999b; Kloiber et al. 2002) to discriminate intraresidual and interresidual correlations, or interresidual CCR rates obtained previously were subtracted from the measured CCR rates (Kloiber and Konrat 2000).

Here, we present novel and simple two-dimensional versions of the quantitative CCR experiments for measuring $\Gamma_{HN,H\alpha C\alpha}(\Phi)$ and $\Gamma_{C',H\alpha C\alpha}(\Phi)$. In order to refocus interresidual $^{2}J_{NC\alpha}$ evolution, the experiments utilize intra-HNCA (Permi 2002; Brutscher 2002; Nietlispach et al. 2002) type coherence transfer to generate multiple quantum (MQ) coherences, $4N_xC'_z(i-1)C^{\alpha}_x(i)$ or $4N_zC'_x(i-1)C^{\alpha}_x(i)$, for obtaining $\Gamma_{HN,H\alpha C\alpha}(\Phi)$ or $\Gamma_{C',H\alpha C\alpha}(\Phi)$, respectively. The contribution from other coherences is also discussed and an appropriate setting of the evolution delays is presented.

Methods

The pulse sequences for the measurement of $\Gamma_{HN,H\alpha C\alpha}(\Phi)$ and $\Gamma_{C',H\alpha C\alpha}(\Phi)$ are shown in Fig. 2a, b, respectively. These pulse sequences are based on intra-HNCA (Permi 2002; Brutscher 2002; Nietlispach et al. 2002) coherence transfer and both experiments consist of pairwise 2D measurements (''reference'' and ''cross'' measurements). During the $2\tau_3$ delay, $^{1}J_{NC'}$, $^{1}J_{NC\alpha}$, and $^{2}J_{NC\alpha}$ couplings evolve simultaneously, and $8N_zC'_z(i-1)C^{\alpha}_z(i)C^{\alpha}_z(i-1)$ coherence is generated at time point ''a.'' Successive units can refocus intraresidual $^{1}J_{C'C\alpha}$ to generate $4N_zC'_x(i-1)C^{\alpha}_z(i)$ at time point ''b.'' In Fig. 2a, successive ^{15}N and $^{13}C^{\alpha}$ 90° pulses ($\varphi 2$ and $\varphi 3$, respectively) can generate $4N_xC'_z(i-1)C^{\alpha}_x(i)$ MQ coherence to measure $\Gamma_{HN,H\alpha C\alpha}$. In Fig. 2b, $4N_zC'_x(i-1)C^{\alpha}_x(i)$ MQ coherence is excited by applying a $^{13}C^{\alpha}$ 90° pulse ($\varphi 3$) to measure $\Gamma_{C',H\alpha C\alpha}$. Successive CCR periods (T) were intrinsically the same as those of the published pulse sequences for measuring $\Gamma_{H\alpha C\alpha,HN}(\Psi)$ and $\Gamma_{H\alpha C\alpha,C'}(\Psi)$ (Chiarparin et al. 1999; Sprangers et al. 2000). After the relaxation period and the additional period ($4\Delta_2$), the $4N_xC'_z(i-1)C^{\alpha}_x(i)$ term is collected directly in the ''reference'' measurement of Fig. 2a. In the ''cross'' measurement, the cross-correlated term $16N_yH^N_zC'_z(i-1)C^{\alpha}_y(i)H^{\alpha}_z(i)$ generated in the relaxation period is converted into $4N_xC'_z(i-1)C^{\alpha}_x(i)$ by $^{1}J_{C\alpha H\alpha}$ evolution during T and $^{1}J_{NH}$ evolution during T and $4\Delta_2$. In the pulse sequence shown in Fig. 2b, the MQ term $4N_zC'_x(i-1)C^{\alpha}_x(i)$ is collected in the ''reference'' measurement, while in the ''cross'' measurement, the $8N_zC'_y(i-1)C^{\alpha}_y(i)H^{\alpha}_z(i)$ term generated by cross-correlated relaxation, is converted into $4N_zC'_y(i-1)C^{\alpha}_x(i)$ by $^{1}J_{C\alpha H\alpha}$ evolution during the relaxation period T. In the ''cross'' measurement of Fig. 2b, in order to suppress the carbonyl chemical shift evolution by moving the two 180° pulses during T, both $^{13}C'$ and $^{13}C^{\alpha}$ 180° pulses between ''a'' and ''b'' are shifted by $\Delta_3 = 2\Delta_1$. Note that this change does not influence

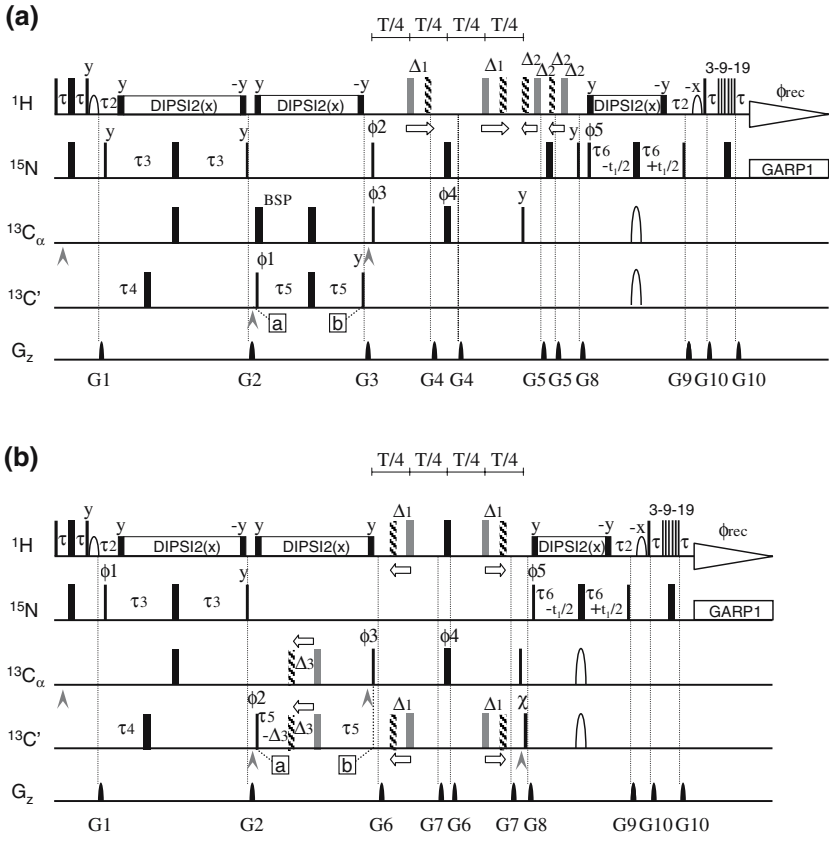

Fig. 2 Pulse scheme for quantification of cross-correlated relaxation rates (**a**) $\Gamma_{HN,H\alpha C\alpha}(\Phi)$ and (**b**) $\Gamma_{C',H\alpha C\alpha}(\Phi)$. Narrow and wide pulses indicate 90° and 180° pulses, respectively. All pulses are applied along the *x*-axis unless indicated. Two open shapes in the middle of $2\tau 6$ indicate a 180° pulse, applied as a single 500 μs adiabatic Chirp pulse (Bohlen and Bodenhausen 1993) which simultaneously inverts $^{13}C^{\alpha}$ and $^{13}C'$ spins. Water flip back is achieved using a H_2O selective sinc pulse and 90° ($\pm y$) pulses flanking the proton decoupling. Suppression of residual water is achieved with a WATERGATE sequence using a 3-9-19 composite pulse (Sklenar et al. 1993). Arrowheads indicate the positions where the ^{13}C carriers ($^{13}C^{\alpha}$ = 54 ppm and $^{13}C'$ = 176 ppm) are jumped. The delays used are τ = 2.25 ms, τ_2 = 5.5 ms, τ_3 = 26 ms, τ_4 = 16.5 ms, τ_5 = 4.5 ms, τ_6 = 20 ms, Δ_1 = 0.89 ms, Δ_2 = 0.49 ms, Δ_3 = 1.78 ms, and T = 28 ms (can be optimized if a C^{α} selective 180° pulse ($\varphi 4$) is applied to refocus the $^1J_{C\alpha C\beta}$ coupling (Yang et al. 1998)). Gray rectangles in the ''reference'' measurement are placed so that scalar couplings are refocused. In the ''cross'' measurement, these pulses are shifted (hatched rectangles) to allow (**a**) evolution under $^1J_{C\alpha H\alpha}$ and $^1J_{NH}$, and (**b**) refocusing of the carbonyl chemical shift and evolution under $^1J_{C\alpha H\alpha}$. The phase cycling is (**a**) $\phi 1 = 4(x), 4(-x)$; $\phi 2 = 2(y), 2(-y)$; $\phi 3 = y, -y$ $\phi 4 = 8(x), 8(y)$; $\phi 5 = y +$ States-TPPI; $\phi_{rec} = x, 2(-x), x, -x, 2(x), 2(-x), 2(x), -x, x, 2(-x), x$; (b) $\phi 1 = 8(y), 8(-y)$; $\phi 2 = x, -x$; $\phi 3 = 2(x), 2(-x)$; $\phi 4 = 4(x), 4(y)$; $\phi 5 = y +$ States-TPPI; $\phi_{rec} = x, 2(-x), x, -x, 2(x), 2(-x), 2(x), -x, x, 2(-x), x; \chi = y$(''reference'') or x (''cross''). Phase corrections for Bloch–Siegert shifts must be optimized for the $\varphi 2$ pulse in pulse scheme (**b**). The duration and strengths of the gradients are G1 = (1 ms, 35 G/cm), G2 = (1 ms, 25 G/cm), G3 = (1 ms, 41 G/cm), G4 = (1 ms, 7 G/cm), G5 = (0.3 ms, 26 G/cm), G6 = (0.3 ms, 18 G/cm), G7 = (0.3 ms, 14 G/cm), G8 = (1 ms, 28 G/cm), G9 = (1 ms, 42 G/cm), and G10 = (1 ms, 21 G/cm)

$^1J_{C'C\alpha}$ evolution. The final ^{15}N constant time t_1 evolution period involves simultaneous refocusing via the $^1J_{NC'}$ and $^1J_{NC\alpha}$ couplings and is followed by a 3-9-19 type WATERGATE refocusing scheme (Sklenar et al. 1993). A longer t_1 for higher spectral resolution can be achieved by using semi-constant time chemical shift evolution (Grzesiek and Bax 1993; Chiarparin et al. 1999).

The new CCR experiments were applied to a sample of 1.7 mM ^{15}N, ^{13}C-labeled human ubiquitin in 95%H_2O/5%D_2O at pH 5.95 on a Bruker Avance 700 spectrometer. All spectra were recorded at 25°C. The CCR relaxation period (T) was set to 28 ms, which can be optimized if a C^{α} selective 180° pulse ($\varphi 4$) is applied to refocus the $^1J_{C\alpha C\beta}$ coupling (Yang et al. 1998). Spectra for ''reference'' and ''cross'' measurements were recorded using 32 and 320 transients per FID, with the corresponding acquisition times of 1.5 and 14 h, respectively. The data were processed and analyzed using NMRPipe (Delaglio et al. 1995). The cross-correlated relaxation rates of both experiments were obtained from the normalized intensity ratios between ''reference'' and ''cross'' experiments in considering the different number of scans: $\Gamma_{HN,H\alpha C\alpha} = -[\tanh^{-1}$

$(I^{\mathrm{cross(a)}}/I^{\mathrm{ref(a)}})]/T; \Gamma_{\mathrm{C'H\alpha C\alpha}} = [\tanh^{-1}(I^{\mathrm{cross(b)}}/I^{\mathrm{ref(b)}})]/T$, where $I^{\mathrm{cross(a)}}$ and $I^{\mathrm{ref(a)}}$ are the normalized resonance intensities of the ''cross'' and ''reference'' measurements of Fig. 2a, respectively, and $I^{\mathrm{cross(b)}}$ and $I^{\mathrm{ref(b)}}$ are the corresponding resonance intensities of Fig. 2b.

Results and discussion

During the $2\tau_3$ delay in Fig. 2, the following eight terms are generated by the evolution of $^1J_{\mathrm{NC'}}$, $^1J_{\mathrm{NC\alpha}}$, and $^2J_{\mathrm{NC\alpha}}$ spin couplings:

$$\mathbf{N}_y \cdot \cos[2\pi J_{\mathrm{NC'}}(\tau_3 - \tau_4)] \cos(2\pi^2 J_{\mathrm{NC\alpha}}\tau_3) \cos(2\pi^1 J_{\mathrm{NC\alpha}}\tau_3) \quad (1)$$

$$2\mathbf{N}_x\mathbf{C'}_z \cdot \sin[2\pi J_{\mathrm{NC'}}(\tau_3 - \tau_4)] \cos(2\pi^2 J_{\mathrm{NC\alpha}}\tau_3) \cos(2\pi^1 J_{\mathrm{NC\alpha}}\tau_3) \quad (2)$$

$$2\mathbf{N}_x\mathbf{C}^{\alpha}_{\mathbf{z}}(i-1) \cdot \cos[2\pi J_{\mathrm{NC'}}(\tau_3 - \tau_4)] \sin(2\pi^2 J_{\mathrm{NC\alpha}}\tau_3) \cos(2\pi^1 J_{\mathrm{NC\alpha}}\tau_3) \quad (3)$$

$$2\mathbf{N}_x\mathbf{C}^{\alpha}_{\mathbf{z}}(i) \cdot \cos[2\pi J_{\mathrm{NC'}}(\tau_3 - \tau_4)] \cos(2\pi^2 J_{\mathrm{NC\alpha}}\tau_3) \sin(2\pi^1 J_{\mathrm{NC\alpha}}\tau_3) \quad (4)$$

$$4\mathbf{N}_y\mathbf{C'}_{\mathbf{z}}\mathbf{C}^{\alpha}_{\mathbf{z}}(i-1) \cdot \sin[2\pi J_{\mathrm{NC'}}(\tau_3 - \tau_4)] \sin(2\pi^2 J_{\mathrm{NC\alpha}}\tau_3) \cos(2\pi^1 J_{\mathrm{NC\alpha}}\tau_3) \quad (5)$$

$$4\mathbf{N}_y\mathbf{C'}_{\mathbf{z}}\mathbf{C}^{\alpha}_{\mathbf{z}}(i) \cdot \sin[2\pi J_{\mathrm{NC'}}(\tau_3 - \tau_4)] \cos(2\pi^2 J_{\mathrm{NC\alpha}}\tau_3) \sin(2\pi^1 J_{\mathrm{NC\alpha}}\tau_3) \quad (6)$$

$$4\mathbf{N}_y\mathbf{C}^{\alpha}_{\mathbf{z}}(i-1)\mathbf{C}^{\alpha}_{\mathbf{z}}(i) \cdot \cos[2\pi J_{\mathrm{NC'}}(\tau_3 - \tau_4)] \sin(2\pi^2 J_{\mathrm{NC\alpha}}\tau_3) \sin(2\pi^1 J_{\mathrm{NC\alpha}}\tau_3) \quad (7)$$

$$8\mathbf{N}_x\mathbf{C'}_{\mathbf{z}}\mathbf{C}^{\alpha}_{\mathbf{z}}(i-1)\mathbf{C}^{\alpha}_{\mathbf{z}}(i) \cdot \sin[2\pi J_{\mathrm{NC'}}(\tau_3 - \tau_4)] \sin(2\pi^2 J_{\mathrm{NC\alpha}}\tau_3) \sin(2\pi^1 J_{\mathrm{NC\alpha}}\tau_3) \quad (8)$$

Among these coherences, the terms (1), (5), (6), ad (7) are eliminated by the second gradient pulse after the ^{15}N evolution delay (G2 in Fig. 2). The terms (3) and (4) are removed by the phase cycling of the first carbonyl 90° pulse. The remaining two terms, (2) and (8), survive by time point ''b'' in Fig. 2 as (A) $4\mathrm{N}_z\mathrm{C}'_y(i-1)\mathrm{C}^{\alpha}_z(i-1)$ and (B) $4\mathrm{N}_z\mathrm{C}'_y(i-1)\mathrm{C}^{\alpha}_z(i)$, respectively. Both of these terms are converted to multiple quantum terms, $4\mathrm{N}_x\mathrm{C}'_z\mathrm{C}^{\alpha}_x$ (Fig. 2a) or $4\mathrm{N}_z\mathrm{C}'_x\mathrm{C}^{\alpha}_x$ (Fig. 2b), during the CCR delay, T. The unfavorable coherence (A) is associated with the CCR rate for the determination of the dihedral angle $\Psi(\Gamma_{\mathrm{H\alpha C\alpha,HN}}(\Psi)$ for Fig. 2a and $\Gamma_{\mathrm{H\alpha C\alpha,C'}}(\Psi)$ for Fig. 2b).

Finally, the two terms are refocused via either $^1J_{\mathrm{NC'}}$ and $^2J_{\mathrm{NC\alpha}}$ or $^1J_{\mathrm{NC'}}$ and $^1J_{\mathrm{NC\alpha}}$ spin couplings during the final ^{15}N constant time t_1 evolution period ($2\tau_6$ delay in Fig. 2). The final coefficients of these terms are written as follows:

$$(2) \Rightarrow \mathbf{N}_y \cdot \sin[2\pi J_{\mathrm{NC'}}(\tau_3 - \tau_4)] \cos(2\pi^2 J_{\mathrm{NC\alpha}}\tau_3) \cos(2\pi^1 J_{\mathrm{NC\alpha}}\tau_3) \sin(2\pi J_{\mathrm{C'C\alpha}}\tau_5) \times \sin(2\pi J_{\mathrm{NC'}}\tau_6) \sin(2\pi^2 J_{\mathrm{NC\alpha}}\tau_6) \cos(2\pi^1 J_{\mathrm{NC\alpha}}\tau_6) \quad (9)$$

$$(8) \Rightarrow \mathbf{N}_y \cdot \sin[2\pi J_{\mathrm{NC'}}(\tau_3 - \tau_4)] \sin(2\pi^2 J_{\mathrm{NC\alpha}}\tau_3) \sin(2\pi^1 J_{\mathrm{NC\alpha}}\tau_3) \sin(2\pi J_{\mathrm{C'C\alpha}}\tau_5) \times \sin(2\pi J_{\mathrm{NC'}}\tau_6) \cos(2\pi^2 J_{\mathrm{NC\alpha}}\tau_6) \sin(2\pi^1 J_{\mathrm{NC\alpha}}\tau_6) \quad (10)$$

The differences in the coefficients for these two terms depend not only on the τ_3 and τ_6 delays, but also on the $^1J_{\mathrm{NC\alpha}}$ and $^2J_{\mathrm{NC\alpha}}$ spin couplings. It is suggested that the size of the $^1J_{\mathrm{NC\alpha}}$ and $^2J_{\mathrm{NC\alpha}}$ spin couplings correlates with the backbone conformation. $^1J_{\mathrm{NC\alpha}}$ values vary between 9 Hz and 13 Hz, while $^2J_{\mathrm{NC\alpha}}$ values vary between 5 Hz and 10 Hz for residues in folded proteins (staphylococcal nuclease and ubiquitin: Delaglio et al. 1991; Wirmer and Schwalbe 2002) and an unfolded protein (ubiquitin: Wirmer and Schwalbe 2002). The error from the unfavorable coherence is estimated from the relative ratio (R-value) of the coefficients of these two terms:

$$R = \frac{\mathrm{term}(A) : 4\mathrm{N}_z\mathrm{C}'_z(i-1)\mathrm{C}^{\alpha}_z(i-1)}{\mathrm{term}(B) : 4\mathrm{N}_z\mathrm{C}'_z(i-1)\mathrm{C}^{\alpha}_z(i)} = \frac{\mathrm{Abs}[\cos(2\pi^2 J_{\mathrm{NC\alpha}}\tau_3) \cos(2\pi^1 J_{\mathrm{NC\alpha}}\tau_3) \sin(2\pi^2 J_{\mathrm{NC\alpha}}\tau_6) \cos(2\pi^1 J_{\mathrm{NC\alpha}}\tau_6)]}{\mathrm{Abs}[\sin(2\pi^2 J_{\mathrm{NC\alpha}}\tau_3) \sin(2\pi^1 J_{\mathrm{NC\alpha}}\tau_3) \cos(2\pi^2 J_{\mathrm{NC\alpha}}\tau_6) \sin(2\pi^1 J_{\mathrm{NC\alpha}}\tau_6)]} \quad (11)$$

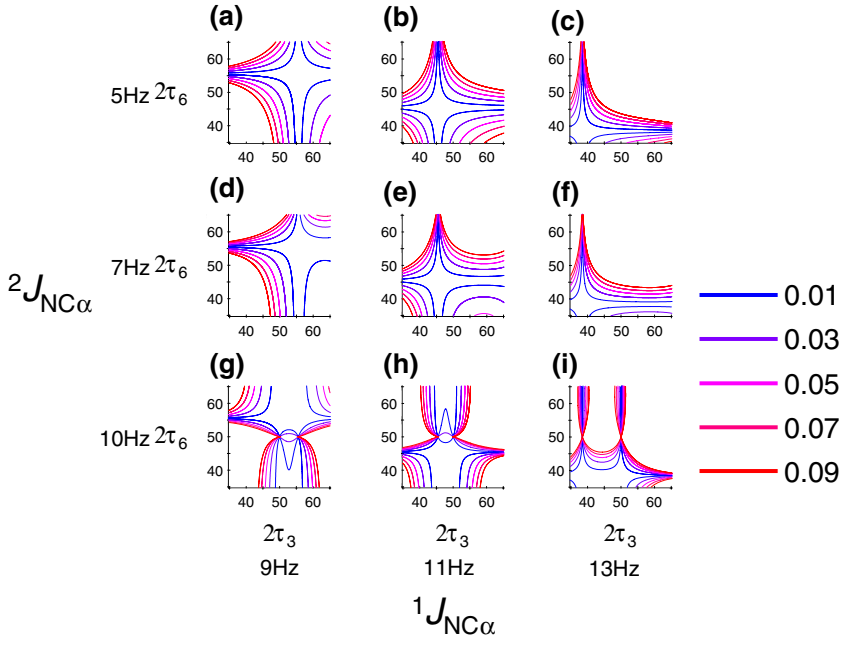

Fig. 3 The relative ratio of the coefficients of the two terms $(4N_zC'_z(i-1)C^{\alpha}_z(i-1)$ and $4N_zC'_z(i-1)C^{\alpha}_z(i))$ as a function of $2\tau_3$ and $2\tau_6$ delays, at different values of $^1J_{NC\alpha}$ and $^2J_{NC\alpha}$. Two-dimensional contour map of *R*-values (Eq. 11), assuming (**a**) $^1J_{NC\alpha} = 9$ Hz and $^2J_{NC\alpha} = 5$ Hz; (**b**) $^1J_{NC\alpha} = 11$ Hz and $^2J_{NC\alpha} = 5$ Hz; (**c**) $^1J_{NC\alpha} = 13$ Hz and $^2J_{NC\alpha} = 5$ Hz; (**d**) $^1J_{NC\alpha} = 9$ Hz and $^2J_{NC\alpha} = 7$ Hz; (**e**) $^1J_{NC\alpha} = 11$ Hz and $^2J_{NC\alpha} = 7$ Hz; (**f**) $^1J_{NC\alpha} = 13$ Hz and $^2J_{NC\alpha} = 7$ Hz; (**g**) $^1J_{NC\alpha} = 9$ Hz and $^2J_{NC\alpha} = 10$ Hz; (**h**) $^1J_{NC\alpha} = 11$ Hz and $^2J_{NC\alpha} = 10$ Hz; (**i**) $^1J_{NC\alpha} = 13$ Hz and $^2J_{NC\alpha} = 10$ Hz. The contours from 0.01 to 0.09 of the *R*-values are plotted with a gradation from blue to red

Figure 3 shows 2D contour maps of the *R*-value as a function of the $2\tau_3$ and $2\tau_6$ delays for several $^1J_{NC\alpha}$ and $^2J_{NC\alpha}$ values. The *R*-value changes drastically with variations in *J* values and/or evolution delays τ_3 and τ_6.

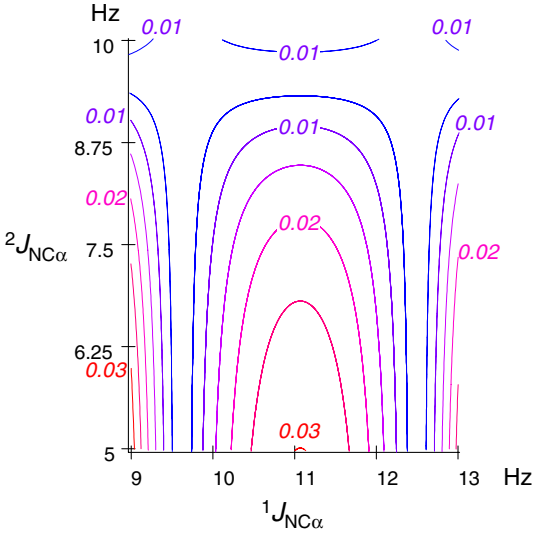

Fig. 4 Two-dimensional contour map of *R*-values (Eq. 11) as a function of $^1J_{NC\alpha}$ and $^2J_{NC\alpha}$ assuming $2\tau_3 = 52$ ms and $2\tau_6 = 40$ ms. The contours from 0.005 to 0.03 of the *R*-values are plotted with a gradation from blue to red

However, if the appropriate combination of τ_3 and τ_6 is selected, the contribution from the unfavorable coherence can be suppressed. Two-dimensional contour maps for $2\tau_3 = 52$ ms and $2\tau_6 = 40$ ms as a function of $^1J_{NC\alpha}$ and $^2J_{NC\alpha}$ values are plotted in Fig. 4. Under these conditions, it is calculated that the maximum value of the unfavorable term (9) is only 3.2% of the desired term (10) for a broad range of $^1J_{NC\alpha}$ and $^2J_{NC\alpha}$ couplings in folded or unfolded proteins.

The newly developed CCR experiments were applied to a sample of 1.7 mM ^{15}N, ^{13}C-labeled human ubiquitin. Figure 5 shows the $\Gamma_{HN,H\alpha C\alpha}(\Phi)$ and $\Gamma_{C',H\alpha C\alpha}(\Phi)$ values as a function of the backbone dihedral angles Φ which were taken from the high resolution X-ray structure for the relevant non-glycine residues (PDB code: 1UBQ). The agreement between experimental CCR rates and theoretical values is comparable to the previously published sequences for the backbone dihedral angle Φ(Pelupessy 1999b; Kloiber et al. 2002; Kloiber and Konrat 2000). The combination of these pairwise CCR rates decreases the number of possible Φ values, analogous to pairwise CCR experiments for the backbone dihedral angle Ψ (Yang and Kay 1998). Moreover, it is reported that a simultaneous interpretation of $\Gamma_{HN,H\alpha C\alpha}(\Phi)/\Gamma_{C',H\alpha C\alpha}(\Phi)$ for Φ angle and $\Gamma_{H\alpha C\alpha,HN}(\Psi)/\Gamma_{H\alpha C\alpha,C'}(\Psi)$

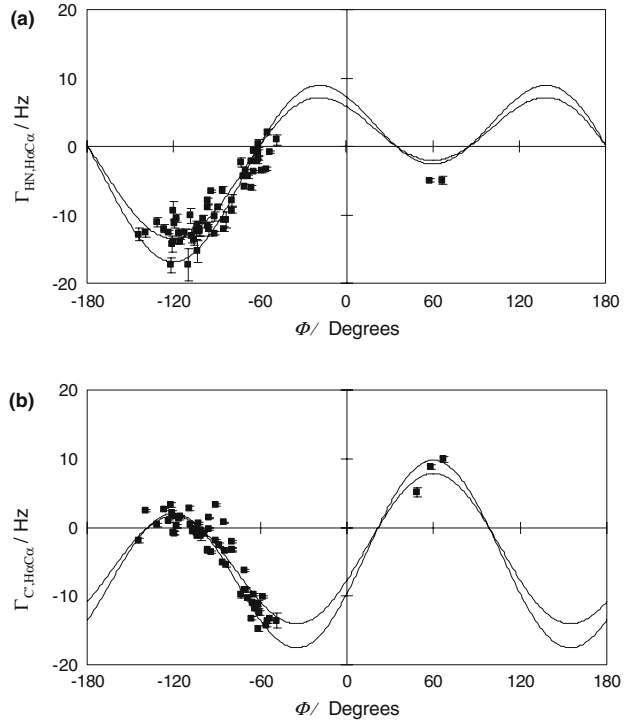

Fig. 5 Correlation between calculated and experimental values of (**a**) $\Gamma_{HN,H\alpha C\alpha}(\Phi)$ and (**b**) $\Gamma_{C',H\alpha C\alpha}(\Phi)$ as a function of the backbone angle Φ, obtained from the X-ray structure of human ubiquitin (PDB code: 1UBQ). The analysis was performed for non-glycine residues, but residues 72–74 were excluded from the analysis because of their flexibility as identified by ^{15}N relaxation (Tjandra et al. 1995). Standard bond lengths and angles (r_{NH} = 1.02 Å and r_{CH} = 1.09 Å) were used for the calculation. The correlation time was assumed to be 4.2 ns. The values of σ_{xx}, σ_{yy}, and σ_{zz} were assumed to be 244, 178, and 90 ppm, respectively (Teng et al. 1992). Error estimations were performed according to the literature (Carlomagno and Griesinger 2000). The two theoretical curves correspond to order parameters S^2 = 1 and 0.8

for Ψ angle along with $\Gamma_{H\alpha C\alpha(i-1),H\alpha C\alpha(i)}$ (Chiarparin et al. 2000) and $^3J_{C'C'}$ scalar coupling achieves the unambiguous determination of protein backbone structure (Kloiber et al. 2002).

Although the CCR experiments presented here can be applied to a protein of <20 kDa by shortening the relaxation delay T with a C^α selective 180° pulse (φ4) (Yang et al. 1998), it would be difficult to apply it to a larger protein (>25 kDa) due to the necessity of the long $J_{NC\alpha}/J_{NC'}$ evolution periods ($2\tau_3$ and $2\tau_6$ delays: 40–50 ms). Rather, a significant benefit is expected when these CCR experiments are applied to peptides that bind weakly to target molecules (transferred cross-correlated relaxation experiments: Blommers et al. 1999; Carlomagno et al. 1999, 2003a, b). This is because not many distance constraints can be obtained from small ligand peptides by transferred NOE experiments and it is difficult to obtain dihedral angle restraints of ligand peptides in the bound state from J-coupling and secondary chemical shift. By utilizing $\Gamma_{HN,H\alpha C\alpha}(\Phi)$ and $\Gamma_{C',H\alpha C\alpha}(\Phi)$ measurements in combination with Ψ angle restraints obtained from $\Gamma_{H\alpha C\alpha,HN}(\Psi)$ and $\Gamma_{H\alpha C\alpha,C'}(\Psi)$ experiments, we can determine high resolution structures of peptides that bind to large molecular weight proteins. Studies to obtain structural information from weakly binding peptides are currently under investigation in our laboratory.

Acknowledgements This work was supported by grants from the New Energy and Industrial Technology Development Organization.

References

Blommers MJJ, Stark W, Jones CE, Head D, Owen CE Jahnke W (1999) Transferred cross-correlated relaxation complements transferred NOE: structure of an IL-4R-derived peptide bound to STAT-6. J Am Chem Soc 121:1949–1953

Bohlen JM, Bodenhausen G (1993) Experimental aspects of chirp NMR-spectroscopy. J Magn Reson A 102:293–301

Brutscher B (2002) Intraresidue HNCA and COHNCA experiments for protein backbone resonance assignment. J Magn Reson 156:155–159

Carlomagno T, Griesinger C (2000) Errors in the measurement of cross-correlated relaxation rates and how to avoid them. J Magn Reson 144:280–287

Carlomagno T, Felli IC, Czech M, Fischer R, Sprinzl M, Griesinger C (1999) Transferred cross-correlated relaxation: application to the determination of sugar pucker in an aminoacylated tRNA-mimetic weakly bound to EF-Tu. J Am Chem Soc 121:1945–1948

Carlomagno T, Blommers MJJ, Meiler J, Jahnke W, Schupp T, Petersen F, Schinzer D, Altmann KH, Griesinger C (2003a) The high-resolution solution structure of epothilone A bound to tubulin: an understanding of the structure-activity relationships for a powerful class of antitumor agents. Angew Chem Int Ed Engl 42:2511–2515

Carlomagno T, Sánchez VM, Blommers MJJ, Griesinger C (2003b) Derivation of dihedral angles from CH–CH dipolar-dipolar cross-correlated relaxation rates: A C–C torsion involving a quaternary carbon atom in epothilone A bound to tubulin. Angew Chem Int Ed Engl 42:2515–2517

Chiarparin E, Pelupessy P, Ghose R, Bodenhausen G (1999) Relaxation of two-spin coherence due to cross-correlated fluctuations of dipole-dipole couplings and anisotropic shifts in NMR of ^{15}N, ^{13}C-labeled biomolecules. J Am Chem Soc 121: 6876–6883

Chiarparin E, Pelupessy P, Ghose R, Bodenhausen G (2000) Relative orientation of $C^\alpha H^\alpha$-bond vectors of successive residues in proteins through cross-correlated relaxation in NMR. J Am Chem Soc 122:1758–1761

Delaglio F, Grzesiek S, Vuister GW, Zhu G, Pfeifer J, Bax A (1995) Nmrpipe – a multidimensional spectral processing system based on unix pipes. J Biomol NMR 6:277–293

Delaglio F, Torchia DA, Bax A (1991) Measurement of ^{15}N–^{13}C J couplings in staphylococcal nuclease. J Biomol NMR 1:439–466

Grzesiek S, Bax A (1993) Amino acid type determination in the sequential assignment procedure of uniformly $^{13}C/^{15}N$-enriched proteins. J Biomol NMR 3:185–204

Kloiber K, Konrat R (2000) Measurement of the protein backbone dihedral angle ϕ based on quantification of remote CSA/DD interference in inter-residue $^{13}C'(i-1)$–$^{13}C^{\alpha}(i)$ multiple-quantum coherences. J Biomol NMR 17:265–268

Kloiber K, Schuler W, Konrat R (2002) Automated NMR determination of protein backbone dihedral angles from cross-correlated spin relaxation. J Biomol NMR 22:349–363

Nietlispach D, Ito Y, Laue ED (2002) A novel approach for the sequential backbone assignment of larger proteins: Selective intra-HNCA and DQ-HNCA. J Am Chem Soc 124:11199–11207

Pelupessy P, Chiarparin E, Ghose R, Bodenhausen G (1999a) Efficient determination of angles subtended by C^{α}–H^{α} and N–H^{N} vectors in proteins via dipole-dipole cross-correlation. J Biomol NMR 13:375–380

Pelupessy P, Chiarparin E, Ghose R, Bodenhausen G (1999b) Simultaneous determination of Ψ and Φ angles in proteins from measurements of cross-correlated relaxation effects. J Biomol NMR 14:277–280

Permi P (2002) Intraresidual HNCA: An experiment for correlating only intraresidual backbone resonances. J Biomol NMR 23:201–209

Reif B, Hennig M, Griesinger C (1997) Direct measurement of angles between bond vectors in high-resolution NMR. Science 276:1230–1233

Sklenar V, Piotto M, Leppik R, Saudek V (1993) Gradient-tailored water suppression for ^{1}H–^{15}N HSQC experiments optimized to retain full sensitivity. J Magn Reson A 102:241–245

Sprangers R, Bottomley MJ, Linge JP, Schultz J, Nilges M, Sattler M (2000) Refinement of the protein backbone angle ψ in NMR structure calculations. J Biomol NMR 16:47–58

Teng Q, Iqbal M, Cross TA (1992) Determination of the ^{13}C chemical-shift and ^{14}N electric field gradient tensor orientations with respect to the molecular frame in a polypeptide. J Am Chem Soc 114:5312–5321

Tjandra N, Feller SE, Pastor RW, Bax A (1995) Rotational diffusion anisotropy of human ubiquitin from ^{15}N NMR relaxation. J Am Chem Soc 117:12562–12566

Wirmer J, Schwalbe H (2002) Angular dependence of $^{1}J(N_i,C_{\alpha i})$ and $^{2}J(N_i,C_{\alpha(i-1)})$ coupling constants measured in J-modulated HSQCs. J Biomol NMR 23:47–55

Yang DW, Kay LE (1998) Determination of the protein backbone dihedral angle ψ from a combination of NMR-derived cross-correlation spin relaxation rates. J Am Chem Soc 120:9880–9887

Yang DW, Konrat R, Kay LE (1997) A multidimensional NMR experiment for measurement of the protein dihedral angle ψ based on cross-correlated relaxation between $^{1}H^{\alpha}$–$^{13}C^{\alpha}$ dipolar and $^{13}C'$ (carbonyl) chemical shift anisotropy mechanisms. J Am Chem Soc 119:11938–11940

Yang DW, Gardner KH, Kay LE (1998) A sensitive pulse scheme for measuring the backbone dihedral angle ψ based on cross-correlation between $^{13}C^{\alpha}$–$^{1}H^{\alpha}$ dipolar and carbonyl chemical shift anisotropy relaxation interactions. J Biomol NMR 11:213–220